Biostatistics and Biometrics
Open Access Journal
ISSN: 2573-2633

Research Article
Volume 10 Issue 4 - September 2022
DOI: 10.19080/BBOAJ.2022.10.555793

Biostat Biom Open Access J

Design and Simulation of the Source (Wiggler) and Medical Beamline of Iranian Light Source Facility (ILSF) for Medical Applications

Homeira Faridnejad*

Department of Physics, East Carolina University, United States

Submission: August 23, 2022; **Published:** September 19, 2022

***Corresponding author:** Homeira Faridnejad, Ph.D. Candidate in Department of Physics, East Carolina University, Howell Science Complex, Greenville, NC 27858, United States

Abstract

To solve the issues, it is crucial to construct a synchrotron accelerator that can later replicate an appropriate medical beamline. There are currently many such accelerators in operation all over the world, and our nation (Iran) is also actively involved in the Sesame project, which is the Middle East's synchrotron being built in Jordan. Additionally, the construction of Iran's accelerator is also anticipated. In this project, we will model the beamline used in radiation and imaging in these accelerators and, in the end, compare it to other accelerators currently on the market for the medical industry (in Canada and the USA) to show and offer a design. By analyzing the achieved data, we can generally say that in analyzing sources for medical beamline, factors such as flux, photon brilliance, and FWHM have considerable impact. These results show that code FLUKA is a powerful tool for simulating medical beamlines. However, such studies in Iran are still in a preliminary stage, and complex parameters must be considered in simulating real beamlines and the results of simulations should be compared with credible experimental data.

Keywords: Photon; FLUKA; Beamline; Wiggler; Medical Applications; Synchrotron Radiation; ILSF

Introduction

By monitoring the uptake and turnover of target-specific radiotracers in tissue, nuclear medicine imaging non-invasively offers functional information at the molecular and cellular level that aids in determining health status [1,2]. These functional activities include tissue metabolism and blood flow, protein-protein interactions, cell-cell interactions, neurotransmitter activity, expression of cell receptors in healthy and unhealthy cells, cell-cell trafficking, tissue invasion, and programmed cell death [3,4]. Nuclear medicine imaging offers a wide range of methods for examining healthy and disease-related states of tissue function and response to therapy by providing information on these processes. Medical imaging and radiotherapy unquestionably play a significant part in the diagnosis and treatment of disorders nowadays [5]. For these images and treatments, systems like standard radiography, mammography, CT scans, accelerators, etc., use a variety of technologies. Since its discovery by Roentgen in 1895 [6], the X-ray has allowed clinicians to display the anatomical conditions of patients' bodies and is one of the rays utilized in such treatments [7].

The benefits of any x-ray imaging system are dependent on the resolution and dose that each patient receives [8, 9]. Synchrotron radiation is one of the techniques used for study and application, among others [7]. Utilizing an accelerator of some kind with a high electron speed produces this radiation (relativity) [10]. The synchrotron radiation produced by this kind of accelerator is used to image the human body with exceptional clarity and resolution while delivering a negligibly high dosage to the patient [5,6,11,12]. Additionally, radiotherapy employs this radiation. Once this radiation is produced, it must pass through devices known as beam lines to increase its strength and radiation quality before it can reach the sample, which is frequently the human body in medical applications [3]. Building a synchrotron and utilizing its radiation for medicinal reasons in Iran is necessary given the challenges in the medical profession that have been mentioned, such as poor image clarity and excessive doses given to patients during diagnosis and treatment [13]. Furthermore, it is crucial for Iranian scholars to investigate and research the many components of this system given Iran's involvement in the Sesame project as well as the plans to construct Iran's national synchrotron accelerator [14]. Evaluating different beam lines in international systems, comparing them with each other, proposing the best design and simulating different stages of it are all of paramount importance and are thus considered in this article [15,16].

Materials and Methods

We estimate the aforementioned curves using the three codes Spectra, Shadow, and XOP while taking into account key source characteristics like flux and photon brilliance in order to achieve the aforementioned objectives for the source [17]. Additionally, after studying the hutches and their necessary components, we determined the component features such as material, thickness, distance from the source, and the distance of each component from the others. We then used the code Fluke to simulate those components, including fixed mask, photon shutter, filter, window, etc., in order to achieve the specified beamline goals [18]. According to the distance from the source, we give the distribution curves of photon dosage and total equivalent dose in the fixed mask and photon shutter. We also estimate the photon flux curve using the energy in the fixed mask [19].

Finally, in table 1. we compare each of the aforementioned curves with the findings of reliable articles on beamlines in the US and Canada in this area in order to validate and evaluate the simulation and present the best appropriate beamline and source [20]. The analysis in this regard showed that the suitable photon flux in the source for medical purpose should be less than 10^{15} ph/s/0.01%bw/mm^2/mrad^2 and photon brilliance should also be less than 10^{20} ph/s/mA/mrad^2/mm^2/0.01%b.w [21] (Table 1).

Table 1: The analysis results include Shadow's calculated photon flux code in medical diagnostic and therapeutic energy.

Resistance level of (FWHM)		Energy resolution power in sample area	Brilliance	Photon flux
Cm horizontal	vertical		ph/s/mA/mrad^2/ mm^2/0.1%b.w	ph/s/0.01%bw/ mm^2/mrad^2
0.00149	0.00143	0.002021	10^{14}-10^{16}	10^{12}-10^{15}

After executing the photon flux ray program, simulating the beam line's components, and applying the FWHM amount obtained from the Shadow code to the source card Fluke [22], we determine the total equivalent dose of a photon in the fixed mask and photon shutter based on the distance from the source. The diameter of the output ray in this simulation is 2.8 centimeters, which is 0.5 cm smaller than the measurement in the pertinent study on the Canadian medical beamline. About 25–40% of the total dose equivalent is represented by the neutron dose equivalent rhythm. The entire dose equivalent in photon shutter has a rhythm of about 1.3 mrem/h.

Methods in simulating beamline

Providing input for the problem:

i. First, we define the surfaces as well as the objects used in the simulation.

ii. Then, by using the surfaces, we make different areas and parts of the problem.

iii. We determine their materials and specifications, and we assign them to different areas.

iv. Now, we define the source in a suitable place.

v. We place the suitable cars to arrange the problem's physics and request (or lack of request) for particle transportation.

vi. We input the output receiver cards and apply classification for them based on the geometric shape, memory size, array dimensions, etc.

Input data in various cards of code Fluka

Source card

In code Fluka, we determine BEAMAXES when needed by using cards BEAM and EAMPOS. By utilizing these cards, we can define spot sources and beams with circular or rectangular cross-sections in different directions. In this project, we used a rectangular source and created mono-energy sources with Gaussian energy distribution around a definable, determined central amount. The energy unit in code FLUKA is GeV, and the source used in this project is set at 3 GeV.

- Energy amount: 3GeV
- Particle type: electron
- Ray shape: Gaussian

FWHM[23]=0.0383, FWHM(y)=0.0058

Ray location cards

- Along X=0 Y=0, Z=610cm

Geometry

The beginning of defining geometry is with GEOBEGIN and its end is with GEOEND. In between, we first have object-defining cards (ending with an END card) and location-defining cards (ending with an END card). This code's geometry is defined by cube, sphere, cone, etc. elements. These geometries begin with the pre-fixed mask with 3 RPP cubes and one TRC cone with specifications [23].

Media card

This card is used to define materials in code FLUKA. We do not need to use this card for the materials available in FLUKA's library. For compound materials, we use COMPUND card to determine the compounds and weight, mass, or volume percentages for each element. Once we have defined the materials in this card, they should be applied to areas that are done by the ASSIGNMA card [24]. In the free format (in which instead of numbers, names are used to determine objects, areas, and materials) when we assign materials to areas, the material of each area must be specified

How to cite this article: Homeira F. Design and Simulation of the Source (Wiggler) and Medical Beamline of Iranian Light Source Facility (ILSF) for Medical Applications. Biostat Biom Open Access J. 2022; 10(4): 555793. DOI: 10.19080/BBOAJ.2022.10.555793

clearly [25]. However, in the fixed format, we can use a range of areas. By using the ASSINGMA card, we define the material and various areas of the problem's geometry. For example, the fixed masks made of copper and collimator made of tungsten, etc.

Results and Discussion

Various medical beamline sections were simulated in this study using the code Fluka, and after much trial and error, we determined the optimal medical beamline by comparing the thicknesses, materials, and separations between the various regions from the source [26,27]. We used the data and output from the US medical beamline to optimize the design and simulations. The photon flux based on energy in the constant mask, the neutron and photon dose distribution in the output and input of the fixed mask, and the photon shutter are pretty near to the output of the US synchrotron and the margin of error is only 3–4%, making this simulation ideal [12,26].

The results of these analyses are presented in the table below, which also includes the calculated photon flux code Shadow within medical diagnostic and treatment energy (80-15keV), photon brilliance, and special resolution of the source based on the amount of width in half of the maximum beamline of FWHM both horizontally and vertically [6].

Flux of wiggler magnet source

As it was explained in chapter 3, in order to calculate photon flux in the source, we should first input the information mentioned in tables 3.2, 3.3, and 3.5 in code Shadow and get find the photon flux curve based on the required photon energy in this project 15-60keV [28] (Figures 1-3).

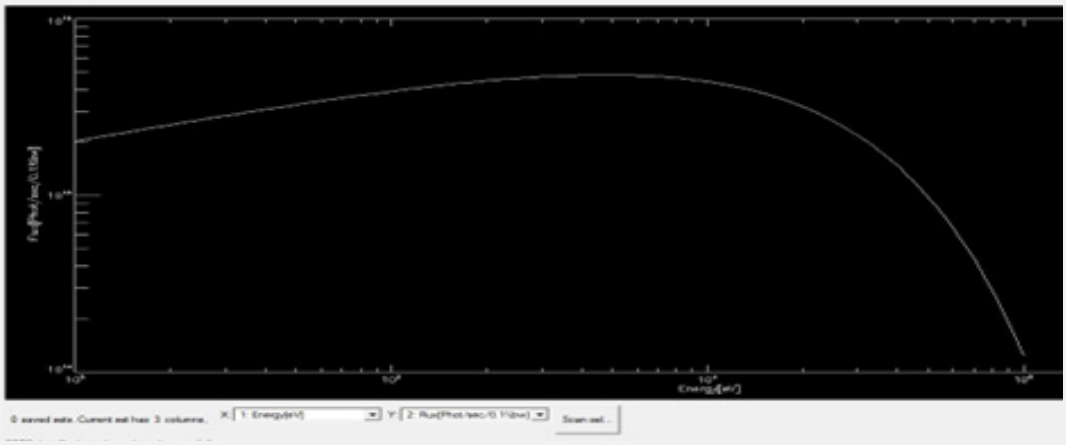

Figure 1: Photon flux curve based on energy (100-10keV) in code Shadow for CLS.

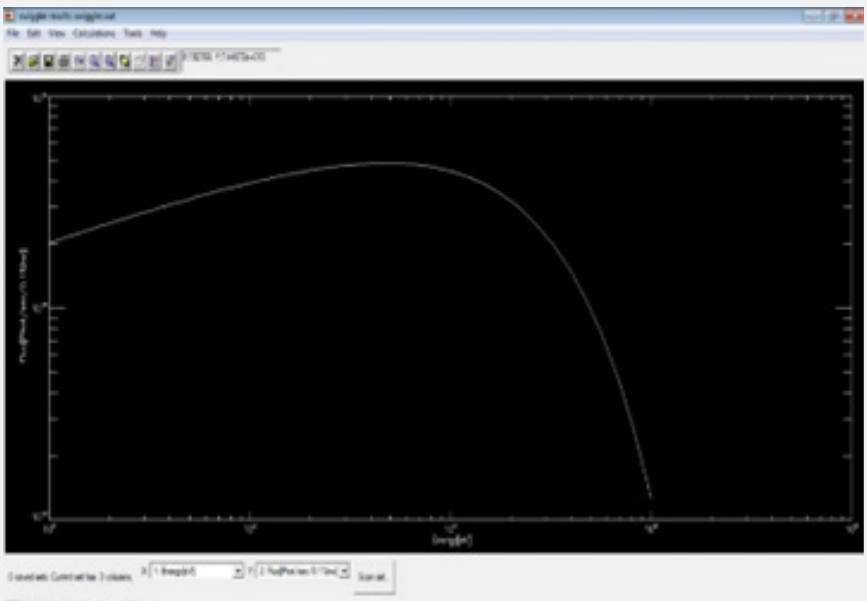

Figure 2: Photon flux based on energy 10-100keV in code Shadow for ILSF.

How to cite this article: Homeira F. Design and Simulation of the Source (Wiggler) and Medical Beamline of Iranian Light Source Facility (ILSF) for Medical Applications. Biostat Biom Open Access J. 2022; 10(4): 555793. DOI: 10.19080/BBOAJ.2022.10.555793

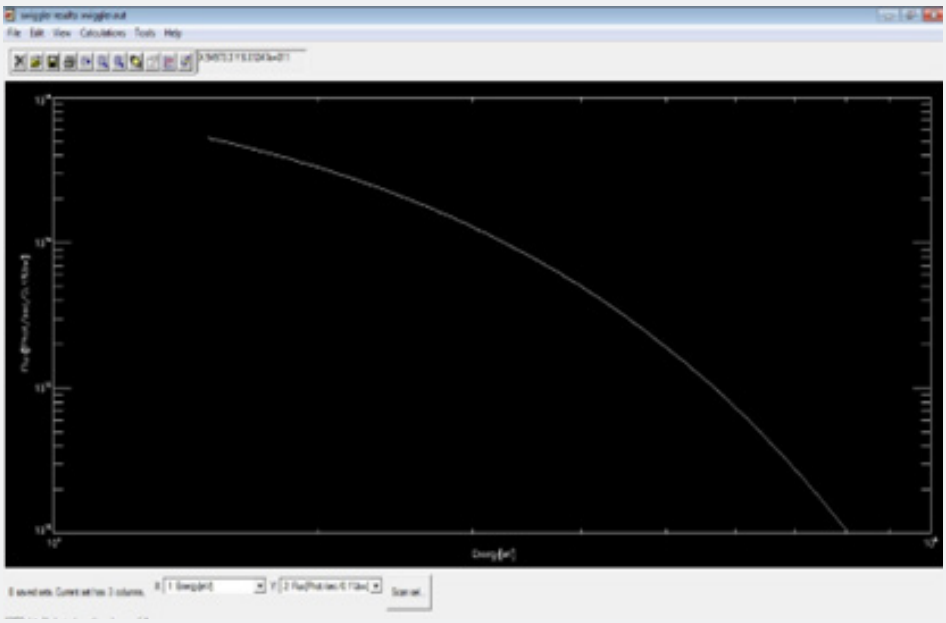

Figure 3: Photon flux curve based on energy 80-15keV in code Shadow for ILSF.

Brilliance in the source by using code Spectra

This curve was drawn and calculated based on information in [Table 3.1] and was calculated in code Spectra [29] (Figure 4).

Energy resolution in sample area in monochromator with code Shadow

We calculated the energy resolution in the sample area in monocheramator by using code Shadow [30]. The distance of the source to monochromator is 18m and the distance of monocheramator to sample is considered as 33m. Energy resolution is calculated within the range of 60-15keV for each energy [31]. As we explained its calculation method explained in chapter 3, the final calculated amount is 0.002021 (Table 2) (Figures 5-8).

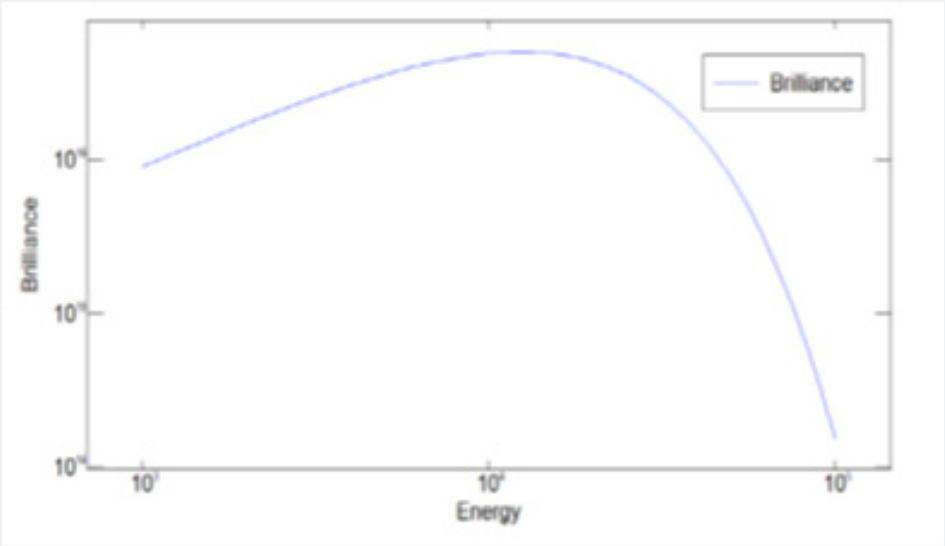

Figure 4: Photon brilliance curve based on energy by using code Spectra.

How to cite this article: Homeira F. Design and Simulation of the Source (Wiggler) and Medical Beamline of Iranian Light Source Facility (ILSF) for Medical Applications. Biostat Biom Open Access J. 2022; 10(4): 555793. DOI: 10.19080/BBOAJ.2022.10.555793

Table 2: Calculating energy resolution and (FWHM) in code Shadow.

FWHM	Energy resolution	Energy range	FWHM	Energy resolution	Energy range
54.25	0.002	28-27	19.97	0.0013	15-16
57.71	0.0020	29-28	26.0086	0.0016	17-16
57.79	0.0019	29-30	31.20	0.0018	17-18
64.122	0.0021	31-30	29.70	0.0016	18-19
64.72	0.0020	32-31	33.20	0.0017	20-19
66.80	0.0020	33-32	33.24	0.0016	21-20
69.49	0.002	33-34	36.074	0.001	22-21
84.23	0.002	35-34	38.833	0.001	23-22
88.47	0.0025	36-35	39.044	0.001	23-24
95.014	0.0026	37-36	49.56	0.002	25-24
100.50	0.0027	37-38	49.84	0.0019	25-26
110.88	0.0029	39-38	52.82	0.002	27-26
182.54	0.003	59-60	110.88	0.0028	39-40
171.60	0.0028	61-60	115.48	0.0028	41-40

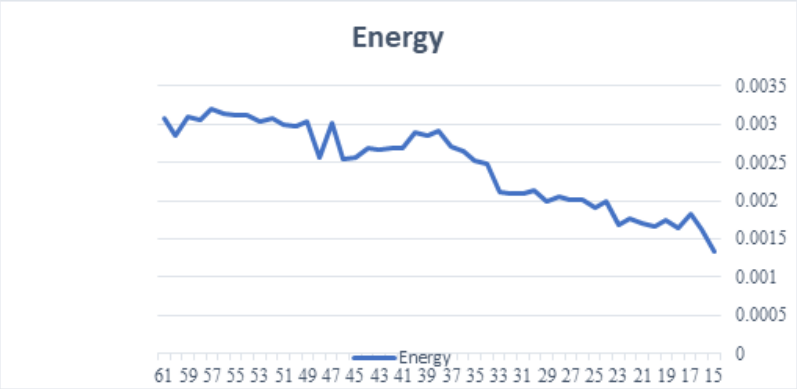

Figure 5: Energy resolution curve based on photon energy in monocheramator in code Shadow.

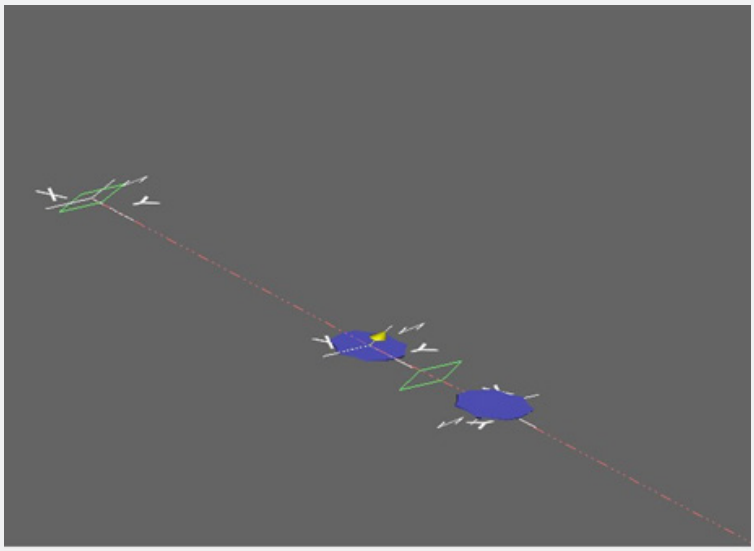

Figure 6: Monocheramator in code Shadow.

How to cite this article: Homeira F. Design and Simulation of the Source (Wiggler) and Medical Beamline of Iranian Light Source Facility (ILSF) for Medical Applications. Biostat Biom Open Access J. 2022; 10(4): 555793. DOI: 10.19080/BBOAJ.2022.10.555793

Figure 7: Calculating (FWHM) in monocheramator in 62keV energy range in code Shadow.

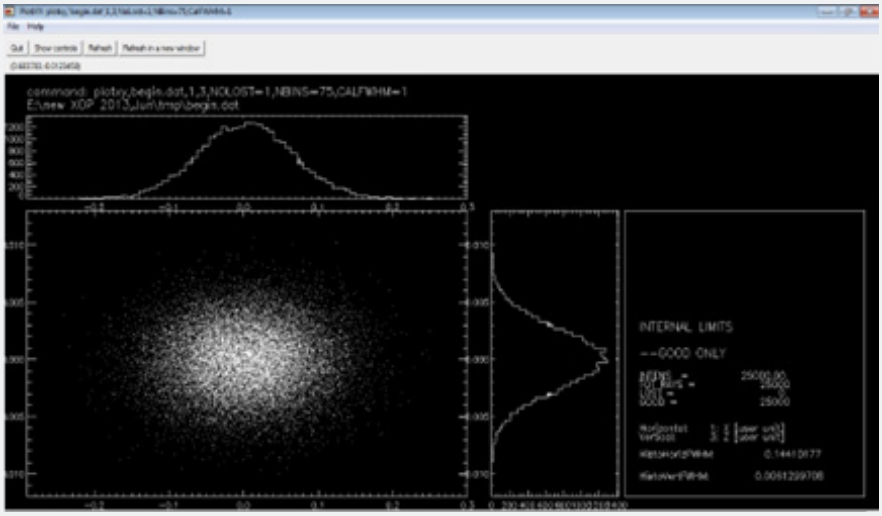

Figure 8: Cross section calculation (FWHM) in source by using code Shadow.

Simulating beamline

For simulation, we need precise information about beamline. This information includes beamline specifications as well as the system's parts [32]. Figures 4.9 and 5.9 are 3d designs of PFM, FM and PhSh that are shown after simulation in code Fluka to depict various device dimensions in Simple Geo software (Figures 9 & 10).

The figures below show simulated geometries [33]. These parts are respectively placed in front-end hutches and include a pre-fixed mask, first mask, photon shutter, (monocheramator is simulated using code Shadow), second fixed mask, safety photon shutter, collimator, and windows 1 and 2 [34]. After it, in light hutch 1 the parts, in order, are primary slit, collimator – fixed mask, (monocheramator is simulated using code Shadow), secondary slit, photon shutter, MRT shutter, and safety shutter. In order to achieve acceptable results, they are a bit larger than the real amount mentioned in pears [35] (Figure 11). The results below show various particle dose distributions and beamline path in various sections.

The rate of dose equivalent distraction in Iran's light source beamline

Figure 4.14 shows the rate of distribution for photon dose equivalent in the exit hole of the fixed mask. As it can be seen, the dose distribution rate on the edges is lower due to the distance from the beamline [36] (Figure 12).

Electron distribution along the beamline parts of Iran's light source (Figures 13 & 14)

Neutron distribution along beamline of Iran's light source (Figure 15)

How to cite this article: Homeira F. Design and Simulation of the Source (Wiggler) and Medical Beamline of Iranian Light Source Facility (ILSF) for Medical Applications. Biostat Biom Open Access J. 2022; 10(4): 555793. DOI: 10.19080/BBOAJ.2022.10.555793

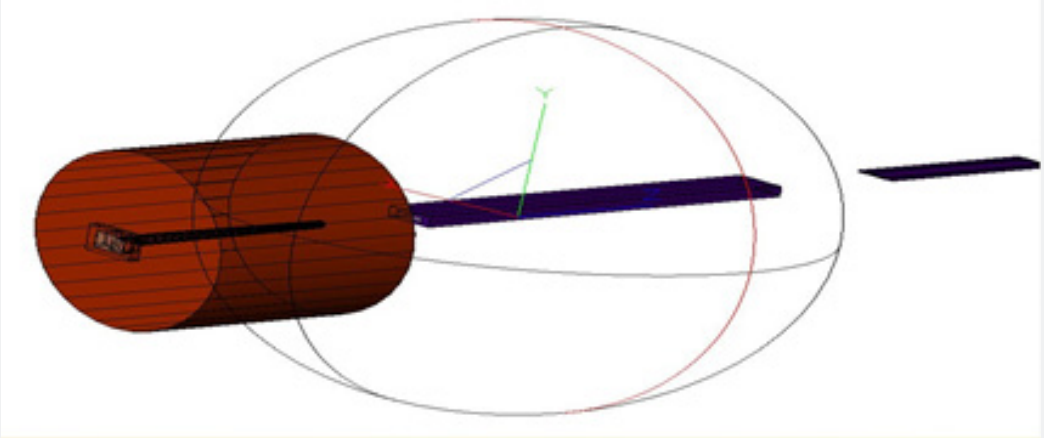

Figure 9: 3D render of PFM, FM and PhSh in Simple Geo.

Figure 10: 3D render of PhSh in Simple Geo.

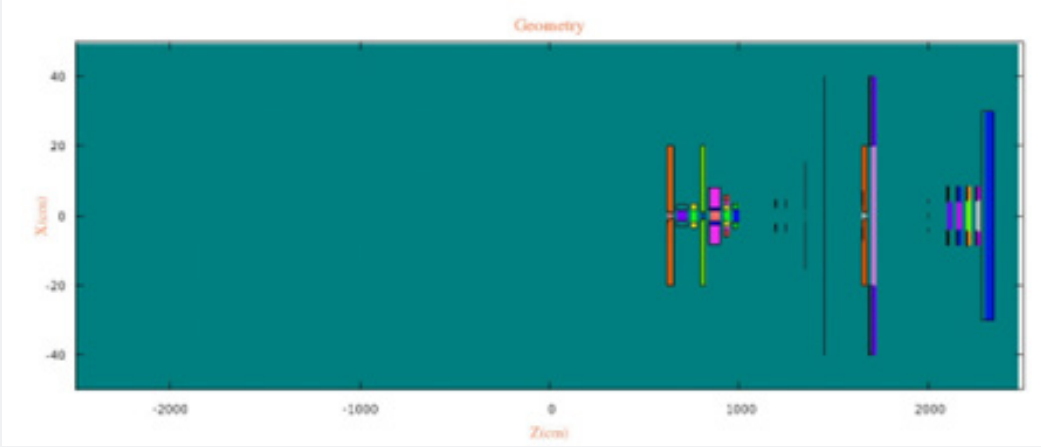

Figure 11: Simulated geometry using Monte Carlo code Fluka.

How to cite this article: Homeira F. Design and Simulation of the Source (Wiggler) and Medical Beamline of Iranian Light Source Facility (ILSF) for Medical Applications. Biostat Biom Open Access J. 2022; 10(4): 555793. DOI: 10.19080/BBOAJ.2022.10.555793

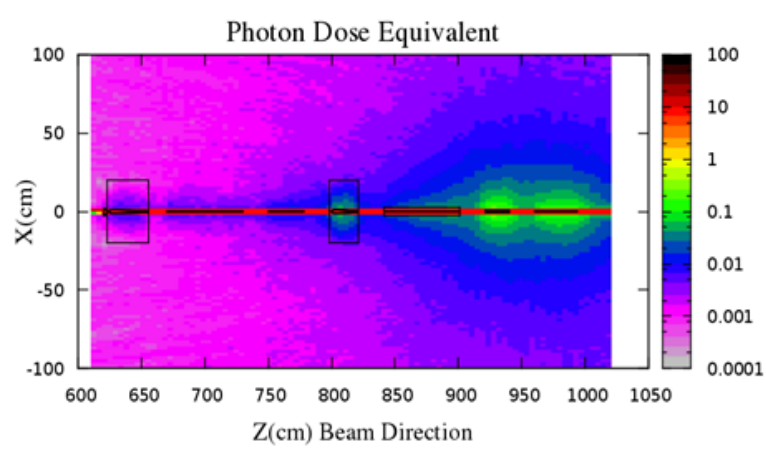

Figure 12: Dose distribution rate in horizontal position on the exit edge of FM based on the distance from source.

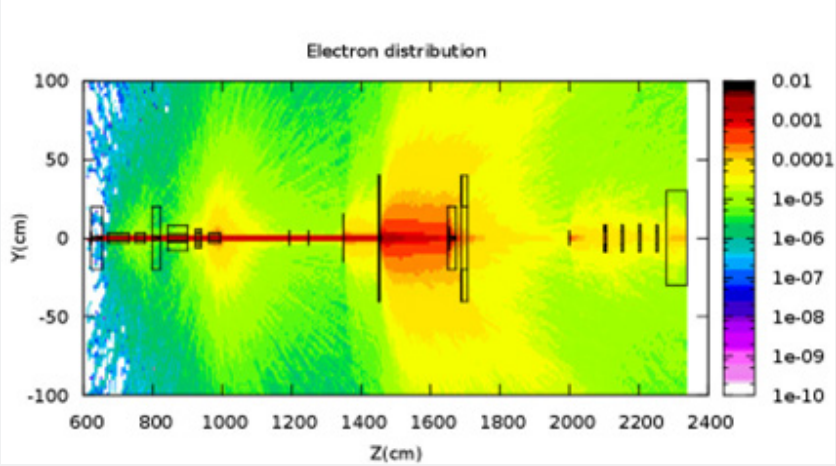

Figure 13: Electron distribution on the vertical axis based on distance from source.

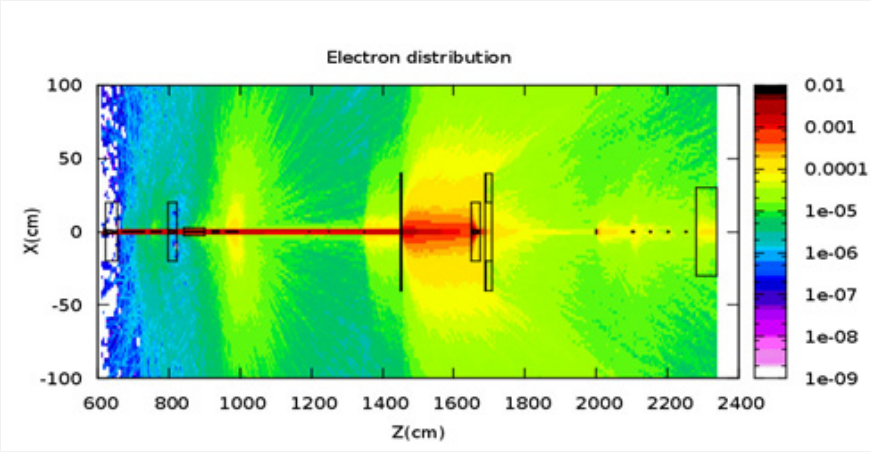

Figure 14: Electron distribution on horizontal axis based on distance from source.

How to cite this article: Homeira F. Design and Simulation of the Source (Wiggler) and Medical Beamline of Iranian Light Source Facility (ILSF) for Medical Applications. Biostat Biom Open Access J. 2022; 10(4): 555793. DOI: 10.19080/BBOAJ.2022.10.555793

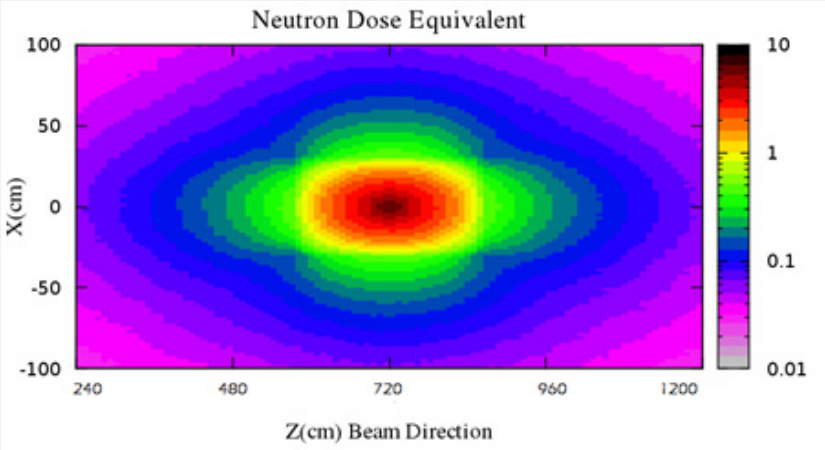

Figure 15: Neutron dose equivalent in perpendicular position on the sheet based on distance from source.

Photon distribution along the devices of beamline in Iran's light source

When the results achieved in this simulation are compared with relevant articles, it becomes clear that the results are close to each other. Dose distribution curves in various areas presented given below **(Figure 16-18)**.

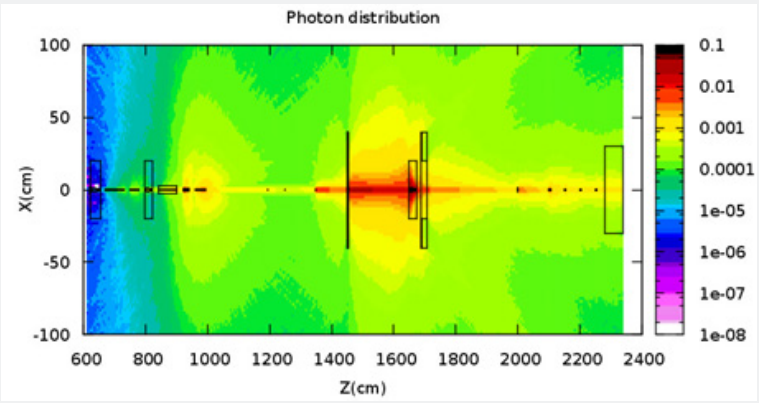

Figure 16: photon distribution on horizontal axis based on distance from source.

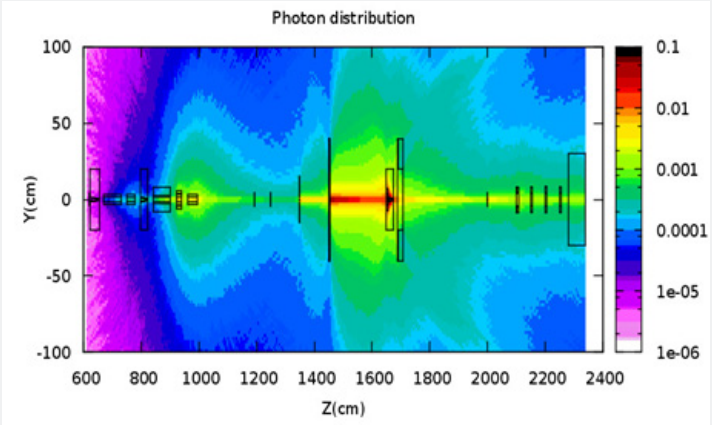

Figure 17: Photon distribution on vertical axis based on distance from source.

How to cite this article: Homeira F. Design and Simulation of the Source (Wiggler) and Medical Beamline of Iranian Light Source Facility (ILSF) for Medical Applications. Biostat Biom Open Access J. 2022; 10(4): 555793. DOI: 10.19080/BBOAJ.2022.10.555793

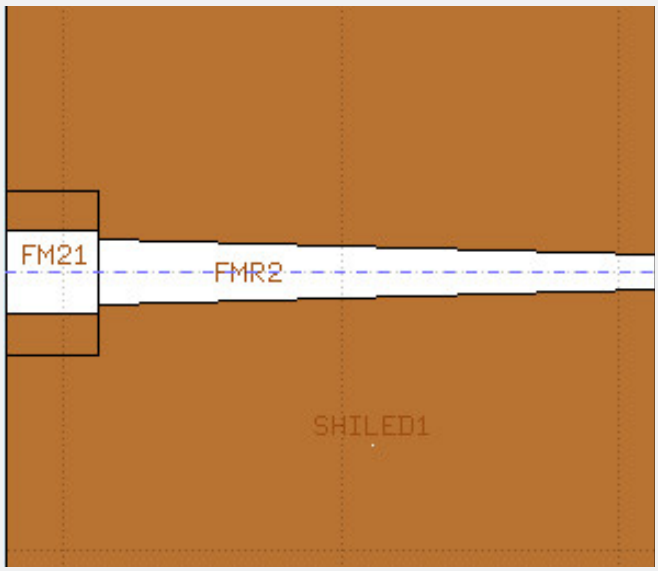

Figure 18: Fixed mas simulated using FLUKA.

Neutron dose distribution in the lower edge of fixed mask

[Figure 4.30] shows the neutron's dose equivalent distribution in a fixed mask environment using ICRP74 calculations; Neutron's weight factor is simulated [37]. Maximum electron beam injection is around 15nC/s in the lower edge of the fixed mask's hole and the maximum neutron dose is less than 100mrem/h at 15nC/s. The neutron dose will not be less than the amount mentioned due to the production of secondary neutrons as a result of a collision with the collimator and photon shutter parts in the front end (Figure 19).

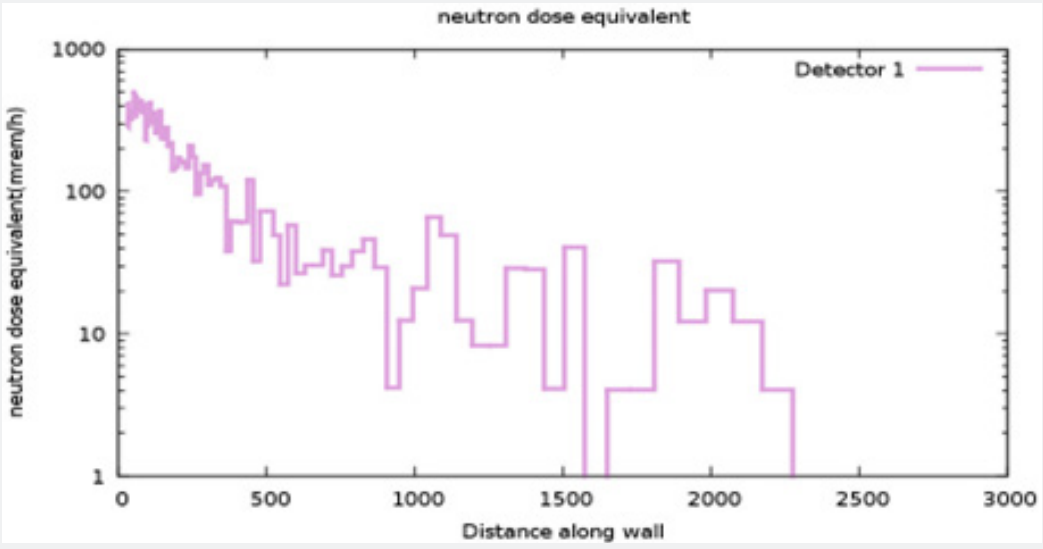

Figure 19: Neutrons' dose equivalent distribution curve in the lower edge of the fixed mask's hole based on distance.

The techniques and systems employed in imaging and treatment, as well as the therapeutic strategies, are essential. We can employ a novel approach to do this by utilizing synchrotron accelerators in medicine, taking into account the benefits and drawbacks indicated in the methods and systems available for x-ray imaging and therapy [38]. The synchrotron radiation produced by this system is devoid of the aforementioned shortcomings of currently used standard systems. Thus, using synchrotron

How to cite this article: Homeira F. Design and Simulation of the Source (Wiggler) and Medical Beamline of Iranian Light Source Facility (ILSF) for Medical Applications. Biostat Biom Open Access J. 2022; 10(4): 555793. DOI: 10.19080/BBOAJ.2022.10.555793

radiation for medical applications can provide the best efficiency while also removing the issues that arise with other imaging and therapy procedures and approaches. The medical beamline under study in this project was recreated utilizing cutting-edge concepts from Canada's synchrotron, and its suitability for usage was assessed by comparison with Canada and US synchrotrons [39].

In order to trust simulation results, they should be compared to a golden standard. That is why we compare them to the results of several papers. Monte Carlo's Fluka simulation was done in various areas of fixed mask and photon shutter to calculate radiations [40]. The dose equivalent rate in this study occurred in photon shutters. The rate of neutron dose equivalent was around 40-25% of rate total dose equivalent rate. The total dose equivalent rate was observed in the photon shutter, and it was calculated to be 1.3 mrem/h. The results of the simulation have small differences from the results of the papers which can be justified as follows: one reason for this divergence is that the size of the dose calculation cells is different. Each dose-depth area in the Fluka simulation is the central part of the cell that is perpendicular to the Z axis [41], which may be the reason for the differences due to not knowing how the distribution calculations were conducted in the papers. Another reason for the causes of differences between the achieved curves with experimental results can be attributed to the differences in the simulated beam such as the cross-section of the beam, etc. [37]. The diameter of the output beam in this simulation is 2.8 centimeters which have a difference of 0.5 centimeters from the one on paper. The reason for this difference may be an error in simulating the descending beam (width multiplied by half of the maximum beam) [42].

Conclusion

In this study, we simulated Iran's light source's beamline for medical purposes. At first, we chose the needed medical light source according to the studies conducted while considering the specifications of Iran's light source machine in CDR (conceptual design report) of 2012. The result of this analysis is choosing a wiggler magnet as the source. The reason is that the energy range for treatment in this research is within 60-15keV and the flux needed for medical applications is less than 1015 ph/s/0.01%bw/mm^2/mrad^2. In addition, the required brilliance in medical applications should again be lower than 1020 ph/s/mA/mrad^2/mm^2/0.1percentage b.w. Considering these requirements and the specifications of Iran's light source machine, this magnet is the best choice for ILSF medical applications. As was mentioned, the calculations for source, flux, photon brilliance, and source FWHM are done using codes XOP and Spectra respectively. To do such calculations, we need critical energy, power parameter, period length, maximum field, beam size, and distribution intensity. The achieved results show that code Fluka is a powerful tool to simulate medical beamlines. That being said, such studies in Iran are still in the initial stages and complex parameters should be considered in simulating a real beamline, and the results of simulations must be compared to credible experimental results.

Acknowledgment

Thanks to Dr. Yousef Naserzadeh for final editing of the article.

References

1. Ghasem H, F Saeidi, and E Ahmadi (2013) Low field low emittance lattice for the storage ring of Iranian Light Source Facility. Journal of Instrumentation 8(02): P02023.
2. Zaka, Ayesha (2021) Energy resolution improvement of a laboratory scale X-ray absorption spectrometer using a position-sensitive detector.
3. Perrot L, R Ollier (2019) Field-map and Beam Transport Calculations of the Magnetic Separator at ALTO Facility at Orsay ISOL. Journal of Physics 1350 012109.
4. A Khaleghi, Z Aghaei, K Mahmoudi, H Haedar, I Imani (2021) A Literature Review of the Efforts Made for Employing Machine Learning in Synchrotrons.
5. Gethmann J (2021) Systematic studies of the beam dynamics with a superconducting damping wiggler at KARA.
6. A J Berejka, M R Cleland, M Walo (2014) The evolution of and challenges for industrial radiation processing. Radiation Physics and Chemistry 94(1): 141-146.
7. Abbasova D, Sunil S (2010) Radiation Processing: Status and Perspectives Dinara Abbasova, Sunil Sabharwal. Ionising Radiation And Mankind 131-151.
8. A P Chernyaev(2012) Nuclear physics-based technologies in medicine. Physics of Particles and Nuclei 43(2): 262-272.
9. Josef Hormes, Henning Lichtenberg, Alexey Maximenko, Alexander Prange, Jacek Szade et al. (2021) A new SOLARIS beamline optimized for X-ray spectroscopy in the tender energy range. Nuclear Instruments and Methods in Physics Research Section B: Beam Interactions with Materials and Atoms 489(1): 6-81.
10. Duke P (2002) Synchrotron radiation: production and properties. Oxford University Press 63(2).
11. S Boucher, E Esarey, C G R Geddes, C Johnstone, S Kutsaev et al. (2022) Transformative Technology for FLASH Radiation Therapy: A Snowmass 2021 White Paper. arXiv preprint arXiv: 2203.11047.
12. Amin Yari, Fereshteh Rajabi Kouchi, Ava Safari Nezhad, Alireza Hadizadeh, Leili Sharif Bakhtiar et al. (2022) Developing an accurate empirical correlation for predicting anti-cancer drugs' dissolution in supercritical carbon dioxide. Scientific Reports 12(1): 01-17.
13. M Umezawa, F Ebina, Y Fujji, K Matsuda (2015) Development of compact proton beam therapy system for moving organs. Hitachi Rev.196-201.
14. Lewis R (1997) Medical applications of synchrotron radiation x-rays. Physics in medicine & biology 42(7): 1213.
15. Luca Brombal, Fulvia Arfelli, Renata Longo, Sandro Donato, Francesco Brun et al. (2021) Motion artifacts assessment and correction using optical tracking in synchrotron radiation breast CT. Medical Physics 48(9): 5343-5355.
16. Ngoc Ton, Steven Machtaler, Arash Panahifar, M Adam Webb, Sheldon Wiebe et al. (2022) Developing a Microbubble-Based Contrast Agent for Synchrotron Multiple-Image Radiography. Molecular Imaging and Biology 24(4): 590-599.
17. Valdivia M, G W Collins, F Conti, F N Beg (2022) Wire, hybrid, and laser-cut X-pinches as Talbot–Lau backlighters for electron density diagnostics. Plasma Physics and Controlled Fusion 64(3): 035011.
18. Hee-Seock Lee, Nam-Suk Jung, Min Ho Kim, Oryun Bae, Hyeon Jae Lee et al. (2018) Assessment of the radiation dose level of the PAL-XFEL Hard X-ray beamlines under accident conditions. Journal of the Korean

How to cite this article: Homeira F. Design and Simulation of the Source (Wiggler) and Medical Beamline of Iranian Light Source Facility (ILSF) for Medical Applications. Biostat Biom Open Access J. 2022; 10(4): 555793. DOI: 10.19080/BBOAJ.2022.10.555793

Physical Society 2018. 73(8): 1061-1067.

19. Su, Peter (2020) Lead chalcogenide thin film materials and processing for infrared optical devices. Massachusetts Institute of Technology.
20. Roy N Platt, Fiona Allan, David Rollinson, Bonnie L Webster, Aidan M. Emery et al. (2022) Genomic analysis of a parasite invasion: Colonization of the Americas by the blood fluke Schistosoma mansoni. Molecular Ecology 31(8): 2242-2263.
21. Anirudh R, Rick Archibald, M Salman Asif, Markus M Becker, Lei Chen et al. (2022) Review of Data-Driven Plasma Science. arXiv preprint arXiv:2205.15832.
22. El-Zein, Ali Abed Ali (2001) Electron and photon interactions with molecules.University College London (United Kingdom).
23. G T Fan, H W Wang, P Kuang, Y X Yang, X G Cao et al. (2021) Collimator system of SLEGS beamline at Shanghai Light Source. Nuclear Instruments and Methods in Physics Research Section A: Accelerators, Spectrometers, Detectors and Associated Equipment. 1013: 165638.
24. Listyana Kumala Sita Nanda, Trisniawati Trisniawati, Mahmudah Titi Muanifah (2022) Development of Android-Based Augmented Reality 3D Card Media for Elementary School Students. AlphaMath: Journal of Mathematics Education 8(1): 88-98.
25. Weinberg, Amir, Nause, Ariel (2022) Beam-line optimization based on realistic electron-optics 3D field-maps implementation provides high-quality e-beam via a dogleg section. Physics of Plasmas 29(6): 063104.
26. Lundberg J, R Woltjer, and B Josefsson (2022) A method to identify investigative blind spots (MIBS): Addressing blunt-end factors of ultra-safe organizations' investigation-work-as-done. Safety Science 154(1):105825.
27. Mozhgan Aghajanzadeh, Mostafa Zamani, Fereshteh Rajabi Kouchi, Farhad Shirini, David Estrada et al. (2022) Synergic Antitumor Effect of Photodynamic Therapy and Chemotherapy Mediated by Nano Drug Delivery Systems. Pharmaceutics 14(2): 322.
28. Vykydal, Zdenek (2012) submitter: Evaluation of Radiation Field Properties with Pixel Semiconductor Detectors Operating in Particle Tracking Mode Freiburg U.
29. Kasen D, R Thomas, and P Nugent (2006) Time-dependent Monte Carlo radiative transfer calculations for three-dimensional supernova spectra, light curves, and polarization. The Astrophysical Journal 651(1): 366.
30. A Gloter, A Douiri, M Tence, C Colliex (2003) Improving energy resolution of EELS spectra: an alternative to the monochromator solution. Ultramicroscopy 96(3-4): 385-400.
31. G T Seidler, D R Mortensen, A J Remesnik, J I Pacold, N A Ball et al. (2014) A laboratory-based hard x-ray monochromator for high-resolution x-ray emission spectroscopy and x-ray absorption near edge structure measurements. Review of Scientific Instruments 85(11): 113906.
32. Krzysztof Genser, Robert Hatcher, Alexander Himmel, Seth R Johnson, Soon Yung Jun (2022) Detector and Beamline Simulation for Next-Generation High Energy Physics Experiments. arXiv preprint arXiv:2203.07614.
33. D Bolst, L T Tran, S Guatelli, N Matsufuji, A B Rosenfeld (2019) Modelling the biological beamline at HIMAC using Geant4. in Journal of Physics Conference series 1154(1): 012003.
34. Omid Faraz, Reza Shahriari, Parsa Movahedi, Ebrahim Nazari Denyani, Mozhdeh Poustchi et al. (2022) Thermodynamic modeling of pharmaceuticals solubility in pure, mixed and supercritical solvents. Journal of Molecular Liquids 353: 118809.
35. Piersimoni P, Piersimoni P, Riccardi C, Pirola M, Ciocca M et al. (2015) Optimization of a general-purpose, actively scanned proton beamline for ocular treatments: Geant4 simulations. Journal of applied clinical medical physics 16(2): 261-278.
36. Christopher M Poole, Liam R J Day, Peter A W Rogers, Jeffrey C Crosbie (2022) A Computerised treatment planning system for synchrotron radiotherapy RMIT University.
37. Mitra Safavi-Naeini, Marissa Kielly, Ilenia D'Adda, Carlo Fiorini, Luca Buonanno et al. (2022) Detection and discrimination of neutron capture events for NCEPT dose quantification. Scientific reports 12(1): 1-14.
38. D Salvato, J Shi, B Baumeister, C Schwarz, C Detavernier et al. (2021) U (Mo) grain refinement induced by irradiation with high energy iodine. Journal of Nuclear Materials 548: 152850.
39. Atcher R W (1979) New radionuclide generator systems for use in nuclear medicine. Argonne National Lab pp. 1-178.
40. Marie-Therese McConnell (2016) A study of the structure and biological activity of the Eranthis hyemalis type II ribosome inactivating protein. Canterbury Christ Church University (United Kingdom).
41. Michael Yannai, Yuval Adiv, Raphael Dahan, Alexey Gorlach, Nicholas Rivera et al. (2022) Demonstration of a Lossless Electron Beam Monochromator in an Ultrafast TEM Using Near-field THz Radiation. CLEO: Science and Innovations.
42. Zhong-Hua Wu, Yun-Peng Liu, Jia-Jun Zhong, Lei Yao, Guang Mo et al. (2022) Silicon PIN photodiode applied to acquire high-frequency sampling XAFS spectra. Nuclear Science and Techniques 33(7): 1-10.

DOI: 10.19080/BBOAJ.2022.10.555793

How to cite this article: Homeira F. Design and Simulation of the Source (Wiggler) and Medical Beamline of Iranian Light Source Facility (ILSF) for Medical Applications. Biostat Biom Open Access J. 2022; 10(4): 555793. DOI: 10.19080/BBOAJ.2022.10.555793